COBEM2015
ABCM Associação Brasileira de Engenharia e Ciências Mecânicas
23rd ABCM International Congress of Mechanical Engineering
December 6-11, 2015, Rio de Janeiro, RJ, Brazil

A NOVEL MODELING METHOD FOR THE INTERFACIAL INSTABILITY OF IMMISCIBLE FLUIDS ALONG DUCTS

Daniel Rodríguez
Department of Mechanical Engineering, Pontifical Catholic University of Rio de Janeiro, Rio de Janeiro, RJ 22453-900, Brazil
danielrodalv84@gmail.com

Abstract. *Most methods used presently in the oil extraction and chemical processing industries for the fast prediction and modeling of interfacial instabilities in confined two-phase flows are based on the so-called one-dimensional two-fluids model, which was developed more than three decades ago. This mechanistic model simplifies the problem by averaging the flow over the cross-section, thus assuming constant velocity profiles and introducing heuristic correlations for the friction factors. Conversely, more fundamental methods for understanding the physics based on variations of the Orr-Sommerfeld equation (e.g. Boomkamp and Miesen (1997)) have been developed less often due to their higher associated computing expenses.*
This paper presents a novel methodology for the computation of confined two-phase flows with interfacial instability. The improved capabilities of present-day computers and algorithms allow us to eliminate the strong simplifications of the two-fluids model and define a problem from first-principles in which the velocity profiles as well as friction factors are computed as part of the solution. A combination of the parabolized Navier-Stokes equations and parabolized stability equations with an interface-capturing scheme analogous to the level-set method are solved using sparse linear algebra and shared-memory parallelization. The proposed method is shown to be able of computing the unsteady velocity field associated with interfacial waves in an oil-water channel flow in few minutes on a laptop computer.

Keywords: *Two-fluid shear flows, Interfacial waves, Parabolized Navier-Stokes equations, Parabolized Stability Equations*

1. INTRODUCTION

Technological problems in which two or more fluids flow concurrently along channels, pipes or ducts with different cross-sections are present in many fields of engineering, like chemical process or oil extraction. The ability of predicting the flow pattern for given configuration and operation conditions is of the utmost importance, due to their significant effect on the global magnitudes of interest for the designer, e.g. pressure losses along duct, drag forces, duct-walls heating, etc. One of such pattern transitions occurs in horizontal or inclined ducts as the flow rate of one or the two phases is gradually increased from relatively low values; the flow then evolves from a steady stratified regime, with smooth interface, towards a wavy stratified regime, in which the interface presents short-wavelength roughness, long waves comparable to the duct cross-section, or a combination of both. If long waves grow enough in amplitude, eventually the cross-section will be bridged by one of the two fluids, and transition may occur to a new pattern, dominated by slugs. Consensus exists in the literature on pointing out interfacial instability as responsible for this transition.

The most generally accepted methods used in the prediction of interfacial instabilities in confined two-phase flows evolved from the one-dimensional two-fluids model (Taitel and Dukler (1976); Lin and Hanratty (1986); Barnea and Taitel (1993)), which assumes a simplified form of the velocity profiles and derives a momentum conservation equation based on averaging the flow properties over cross-sections. The reason of the success of this method relies on the necessity of introducing heuristic correlations for the wall and interfacial friction factors which, once calibrated with experiments, can deliver reasonable predictions in a great variety of flows. On the other hand, methods derived from first-principles for understanding the physical processes associated with interfacial instabilities, like those presented by Kuru *et al.* (1995) or Boomkamp and Miesen (1997), have not been applied in the same degree as the one-dimensional two-fluids model, due to their higher computational expenditure.

The present paper presents a novel methodology for the computation and study of interfacial instability on stratified flow along ducts. The improved capabilities of present computers along with numerical techniques developed over the last decade (e.g. Gennaro *et al.* (2013)) enable the extension, to two-phase flow problems, of methods for the efficient computation of steady or time-averaged flows and of the spatial evolution of flow instabilities, which were originally devised for single-phase flows. These methods share a parabolic integration of the governing equations along the streamwise direction and can be coupled in a simple manner, resulting into very fast computations compared to time-marching computations (Gada and Sharma (2012)) that compute analogous flows.

The rest of the paper is organized as follows. Section 2 outlines the governing equations and modeling methodology presented. It consist of adaptations of the Parabolized Navier-Stokes (PNS - Anderson *et al.* (1984)) approach for the mean flow and the nonlinear Parabolized Stability Equations (PSE -Herbert (1997)) approach for the fluctuations, to two-phase flows confined on ducts of, in principle, arbitrary cross-section. Section 3 briefly summarizes the numeric and algorithmic methods used in the solution. Some validations and demonstrative results are presented in section 4, where the simple two-dimensional oil-water channel flows of Gada and Sharma (2012) are addressed for comparison. Some remarks and the improvements that are currently underway are mentioned in Section 5.

2. MATHEMATICAL MODELING

The mathematical model for the confined two-phase flow within pipes is based on the complete Navier-Stokes equations in differential form, as opposed to mechanistic models (Taitel and Dukler (1976); Lin and Hanratty (1986); Barnea and Taitel (1993)) based on an integral evaluation of the conservation equation for axial momentum. A single-fluid method along with an interface-capturing level-set approach is used here to describe the fluid motion, as described next.

Equations are non-dimensionalized using the following magnitudes: a length characteristic of the duct cross section, e.g. the channel width or pipe diameter D^*; a characteristic velocity in one of the phases U_1^*, typically the less dense one; the corresponding density and molecular viscosity in the same phase, ρ_1^* and μ_1^*; a characteristic convection time D^*/U_1^*; and the dynamic pressure on phase 1, $\rho_1^* U_1^{*2}$. Denoting the gravity acceleration by g^* and the surface tension coefficient between the two phases by σ^*, the following dimensionless quantities are formed:

$$\chi = \frac{\rho_2^*}{\rho_1^*}, \quad \eta = \frac{\mu_2^*}{\mu_1^*}, \quad Re = \frac{\rho_1^* U_1^* D^*}{\mu_1^*}, \quad We = \frac{\rho_1^* U_1^{*2} D^*}{\sigma^*} \quad \text{and} \quad Fr = \frac{U_1^*}{\sqrt{g^* D^*}}. \tag{1}$$

In this dimensionless form, the momentum and mass conservation equations can be written as

$$\rho\frac{\partial \mathbf{v}}{\partial t} + \rho \mathbf{v}\cdot\nabla\mathbf{v} = -\nabla p + \frac{1}{Re}\nabla\cdot(2\mu\mathbf{D}) + \frac{1}{We}\mathbf{T} + \frac{1}{Fr^2}\mathbf{g}, \quad \text{and} \quad \nabla\cdot\mathbf{v} = 0, \tag{2}$$

where $\mathbf{D} = (\partial u_i/\partial x_j + \partial u_j/\partial x_i)/2$ is the velocity gradient tensor, $\mathbf{T}$ is a volume force modeling the surface tension and $\mathbf{g}$ is the unitary vector pointing in the direction of gravity.

A level set method (Sussman *et al.* (1994)) is employed here in order to capture the fluid interface and track its deformation without incurring in heavy computational costs. A scalar function ϕ is defined such that $\phi = 0$ at the interface, $\phi > 0$ at phase 1 and $\phi < 0$ at phase 2. The evolution of the scalar level-set function is governed by

$$\frac{\partial \phi}{\partial t} + \mathbf{v}\cdot\nabla\phi = 0. \tag{3}$$

After introduction of ϕ, the density and viscosity spatial distributions are expressed as

$$\rho = H(\phi) + \chi(1 - H(\phi)), \quad \text{and} \quad \mu = H(\phi) + \eta(1 - H(\chi)), \tag{4}$$

where H is the Heaviside function.

Provided that $\phi = 0$ defines the interface location, the interface local normal vector, curvature and surface tension are defined as

$$\mathbf{n} = \frac{\nabla\phi}{|\nabla\phi|}, \qquad \kappa(\phi) = \nabla\cdot\left(\frac{\nabla\phi}{|\nabla\phi|}\right), \quad \text{and} \quad \mathbf{T} = \kappa(\phi)\delta(\phi)\mathbf{n} = \delta(\phi)\nabla\cdot\left(\frac{\nabla\phi}{|\nabla\phi|}\right)\frac{\nabla\phi}{|\nabla\phi|}, \tag{5}$$

where the Dirac delta function δ has been used. The fluid flow described by equations (2), and (3) is represented in vector form as $\mathbf{q} = [\mathbf{v}\ p\ \phi]^T$, and is a function of the three spatial directions (x denoting the axial direction and y and z denoting the cross-sectional ones) and time t. Following Reynolds decomposition, the flow is divided into a time-independent *mean* flow $\bar{\mathbf{q}}$ and a fluctuation component $\mathbf{q}'$:

$$\mathbf{q} = \bar{\mathbf{q}}(\mathbf{x}) + \mathbf{q}'(\mathbf{x}, t). \tag{6}$$

The mean flow $\bar{\mathbf{q}}$ can represent a steady solution of the governing equations or a time-averaged flow obtained from time-accurate numerical simulations, Reynolds-averaged Navier-Stokes (RANS) simulations or experimental measurements. Upon substitution of equation (6) on the governing equations (2), and (3), two systems of equations are obtained respectively for the mean flow and fluctuations. These two systems are coupled by both linear and nonlinear interactions, and its accurate solution would require of large numerical computations (Gada and Sharma (2012)). The characteristics of the flow under consideration can be exploited in order to introduce simplifications in the governing equations, that allow us to obtain solutions in a very efficient manner. These simplifications are discussed next.

2.1 TURBULENT FLOW DECOMPOSITION AND LARGE SCALES

Flows of engineering significance are characterized by relatively high Reynolds numbers, so that turbulence is inherent to the dynamics of all spatial and temporal scales. However, most turbulent flows exhibit large-scale organizations of the fluid motion, that are coherent over scales (spatial and temporal) of the order of the integral scales, that is, characteristic of the mean properties of the flow. Existence and dominance of large-scale turbulence structures has been documented for a variety of single-phase flows (Holmes *et al.* (1996)), and a mathematical theory was put forward for the analysis of these structures as originated by the instability of the turbulent time-averaged flow. The *triple-decomposition* was originally proposed by Reynolds and Hussain (1972), that modified Reynolds decomposition (6) by separating the fluctuations into *coherent* (or large-scale) and in-coherent or random fluctuations

$$\mathbf{q} = \bar{\mathbf{q}}(\mathbf{x}) + \tilde{\mathbf{q}}(\mathbf{x}, t) + \mathbf{q}''(\mathbf{x}, t). \tag{7}$$

Again, linear and nonlinear interactions are possible amongst the three different components. In those flows in which coherent structures are well defined and much more energetic than the random turbulent fluctuations, the dynamics of the large scales can be expected to be governed mainly by its interaction with the mean flow, while the smaller turbulent scales can be assumed to act as an energy dissipation mechanism. From the modeling point of view, the random turbulence only needs to be accounted for as an energy sink acting on both the mean flow and the large-scales structures, and then classical eddy viscosity models like those used in RANS computations may provide a good closure for the equations.

Modeling the interactions between the mean flow and the large-scale structures is necessarily more involved. Large-scale fluctuations are originated, in most cases, by linear instability processes that lead to a transfer of energy from the mean flow to the fluctuations (Reynolds and Hussain (1972); Boomkamp and Miesen (1997)). On the other hand, finite-amplitude fluctuations can attain kinetic energy levels comparable to the mean flow, and then have the potential to effect mean flow distortions via nonlinear interactions. This nonlinearities need to be accounted for explicitly in the model equations.

Interfacial instability of immiscible flows is one example of flows in which large scale structures (the interface undulations) are present and distinguishable from the small scale turbulence. Wall-turbulence models have been shown to deliver good predictions of the turbulent shear stresses at the duct walls and reproduce the main features of the turbulent mean flow. On the other hand, large scale structures are generated by interfacial instability processes and then modified by nonlinear interaction. The nonlinear interactions determine if the growth of the interfacial wave will saturate, resulting into a wavy stratified flow, or otherwise the wave amplitude will grow until the interface reaches the upper duct wall, bridging the cross-section and producing a proto-slug, and possibly transition to slug regime (Lin and Hanratty (1986)).

In this paper, the effect of small-scale random turbulence fluctuations is neglected, in order to simplify the equations employed and for the sake of cleanliness of exposition. However, scalar models based on the Boussinesq approximation can be implemented in a trivial manner without increasing significantly the complexity of the model or the computational cost.

2.2 PARABOLIZATION OF THE EQUATIONS

The geometrical configuration along with the flow characteristics allows us to introduce the following simplification: the mean flow properties are slowly varying along the axial $x-$direction. In the time-averaged flow, changes along the axial direction appear due to the axial pressure gradient, that affects the flow globally, and due to molecular and turbulent diffusion, which are proportional to the Reynolds number. Without a detailed analysis of the turbulent diffusion scales, let us assume that the axial variations of the mean flow properties are very slow compared to those on the duct cross-section: $\partial/\partial x \ll \partial/\partial y, \partial/\partial z$. Then, we can introduce a *slow* variable $X = \gamma x$ with $\gamma \ll 1$, such that $\partial/\partial X \sim \partial/\partial y, \partial/\partial z$.

Introducing this separation of scales in the axial momentum equation, and taking orders of magnitude in the viscous terms, we observe that the terms associated with axial derivatives are negligible with respect to cross-sectional terms. We find analogous relations in the other momentum equations. The consequence is that the terms involving second-order derivatives on x can be neglected, and we arrive at a system of equations with only first-order derivatives on x. This simplification is referred to as the weakly non-parallel flow approximation.

The governing equations for the mean flow are time-independent, and can be re-casted as a parabolic problem whose solution is obtained by marching the equations downstream; this approach, related but not identical to the boundary-layer approximation, has been used extensively for subsonic and supersonic single-phase flows and is known as Parabolized Navier-Stokes (PNS) equations (Anderson *et al.* (1984)). The present paper is its first application to confined multiphase flow, to the author's best knowledge. The equations governing the fluctuations are not time-independent, but can be transformed to the frequency domain without loss of generality by introducing Fourier modes. In doing so, the equations governing the dynamics of each frequency can be parabolized based on similar arguments to those used for the mean flow, resulting into the nonlinear Parabolized Stability Equations (PSE) (Herbert (1997)). The PNS and PSE system of equations must be marched together: the mean flow quantities enter linearly in the coefficients of the PSE, while the fluctuations modeled by PSE generate, through nonlinear interactions, a forcing term that modifies the mean flow. The present paper focuses on describing the modeling strategy rather than showing new physical results; consequently a simple two-dimensional channel configuration is addressed in what follows.

2.3 PARABOLIZED NAVIER-STOKES EQUATIONS FOR MULTIPHASE FLOW ON DUCTS

The system of equations (2), and (3) is particularized now for two-dimensional flow. Following from the parabolization discussed above, viscous terms comprising second axial derivatives as well as time-derivative terms are neglected. However, the system of equations is not fully parabolized yet. Two possible sources of ellipticity exit, that are discussed now.

The first source is related to the tension surface. In two-dimensions, the interface curvature is

$$\kappa(\bar{\phi}) = \left(\bar{\phi}_x^2\bar{\phi}_{yy} + \bar{\phi}_y^2\bar{\phi}_{xx} - 2\bar{\phi}_x\bar{\phi}_y\bar{\phi}_{xy}\right)/|\nabla\bar{\phi}|^3 \tag{8}$$

where subscripts denote partial differentiation. This expression involves second derivatives on x and would prevent us from marching the problem downstream. However, the weakly non-parallel flow hypothesis is invoked again for $\bar{\phi}$: $\bar{\phi}_x, \bar{\phi}_{xy} \sim \gamma, \quad \bar{\phi}_{xx}, \bar{\phi}_x^2 \sim \gamma^2 \ll 1$. Consequently, we can neglect the direct influence of the surface tension in the computation of the mean flow. This is a reasonable approximation, as the mean location of the interface is smooth and has slow variations along the axial direction. The surface tension originated by interface oscillations will play a role in an indirect manner through the nonlinear interactions.

The second source of ellipticity is related to axial pressure gradients. The bulk pressure gradient being responsible for the motion of the flow within the duct, there is no simplification possible. Within the weakly non-parallel hypothesis, the axial and cross-sectional pressure gradients are associated with balancing of different forces acting on the dynamics. Axial velocity and pressure gradient are of a higher magnitude and dominate over cross-section dynamics, and are related to the *primary flow*, i.e. the bulk mass transfer along the pipe or duct. Cross-sectional velocities and pressure gradients are associated with *secondary* flows, or local adaptations of the velocity profile, that are much weaker than those corresponding to the primary one. As a consequence, we can divide the pressure in two components, $\bar{p} = \bar{P}(x) + \bar{p}(x, y)$, where $\bar{P}$ is the bulk pressure and the secondary pressure $\bar{p}$ is a lower order correction on cross sections, and $\partial\bar{p}/\partial x \ll \partial\bar{P}/\partial x$.

Most applications of PNS in the literature consider open geometries where the external (inviscid) pressure gradient $\bar{P}_x$ is known and imposed directly on the equations as a known function of the axial position. In internal flows, the quantity that is naturally known and controlled in experiments is the mass flow rate, or in the case of two immiscible fluids, the mass rate of each phase:

$$G_1 = \int_A \bar{\rho}\bar{u}H(\bar{\phi})\,\mathrm{d}A, \quad \text{and} \quad G_2 = \int_A \bar{\rho}\bar{u}(1 - H(\bar{\phi}))\,\mathrm{d}A. \tag{9}$$

The primary axial pressure gradient should be obtained as part of the solution in order to verify conservation of the individual phases. The axial pressure gradient $\bar{P}_x$ is then iterated at each axial step of the integration using a Newton iteration, until the conditions (9) are satisfied. The cross-sectional gradients of $\bar{p}$ does not affect the parabolization of the equations.

Finally, the system of equations to be solved for the mean flow is:

$$\bar{\rho}\bar{u}\bar{u}_x + \bar{\rho}\bar{v}\bar{u}_y = -\bar{P}_x + \frac{1}{Re}\left[\frac{\partial}{\partial y}(\bar{\mu}\bar{u}_y)\right] - \frac{\bar{\rho}\sin\beta}{Fr^2} + \bar{F}^x, \tag{10}$$

$$\bar{\rho}\bar{u}\bar{v}_x + \bar{\rho}\bar{v}\bar{v}_y = -\bar{p}_y + \frac{1}{Re}\left[\frac{\partial}{\partial y}(\bar{\mu}\bar{v}_y)\right] - \frac{\bar{\rho}\cos\beta}{Fr^2} + \bar{F}^y, \tag{11}$$

$$\bar{u}_x + \bar{v}_y = \bar{F}^c, \tag{12}$$

$$\bar{u}\bar{\phi}_x + \bar{v}\bar{\phi}_y = \bar{F}^l. \tag{13}$$

The terms $\bar{F}^x, \bar{F}^y, \bar{F}^c$ and $\bar{F}^l$ arise due to nonlinear interactions with the fluctuations. The closure of the equations requires of prescribing adequate boundary conditions at the duct walls, and of one inlet flow that satisfies the equations. No-slip conditions are imposed at the walls, along with a compatibility condition for the pressure and homogeneous Neumann boundary conditions for $\bar{\phi}$. The inlet profile can be modified according to the details of the particular set-up.

2.4 PARABOLIZED STABILITY EQUATIONS FOR MULTIPHASE FLOW ON DUCTS

The equations governing the fluctuations are Fourier-transformed to the frequency domain. The fluctuating flow component can be written, without loss of generality, as a sum of Fourier modes characterized by their frequencies, $\mathbf{q}' = \sum_m \tilde{\mathbf{q}}_m \exp(-\mathrm{i}\omega_m t)$. The separation in scales resulting from the weakly non-parallel flow assumption is also invoked for the fluctuations, which can be decomposed into two components

$$\tilde{\mathbf{q}}_m(x, y) = A_m(x)\hat{\mathbf{q}}_m(x, y), \tag{14}$$

where the *amplitude factor* A_m is given by

$$A_m(x) = \exp\left(\mathrm{i}\int_{x_0}^{x} \alpha_m(\xi)\mathrm{d}\xi\right). \tag{15}$$

Each, shape function $\hat{\mathbf{q}}_m$ is associated with an axial wavenumber α_m and frequency ω_m. The amplitude factor comprises the fast oscillations associated with the wave-like behavior implicitly assumed for the fluctuations. While α_m remains a slowly varying function of the axial coordinate x, the changes in A_m happen in distances much smaller than those characteristic of the mean flow variations. The shape function, $\hat{\mathbf{q}}_m$ also has a slow variation on the axial direction. Provided that α_m and $\hat{\mathbf{q}}_m$ evolve downstream in the scale of the slow variable X, the simplifications discussed above, i.e. $\partial^2\hat{\mathbf{q}}_m/\partial x^2 \ll 1$, and $\mathrm{d}^2\alpha_m/\mathrm{d}x^2 \ll 1$, also hold here and justify neglecting these terms in the governing equations. Note that only the second-order axial derivatives of the shape function have been neglected, but first and second-order derivatives of the fluctuations do not vanish and take the form

$$\frac{\partial\tilde{\mathbf{q}}_m}{\partial x} = \left[\mathrm{i}\alpha_m\hat{\mathbf{q}}_m + \frac{\partial\hat{\mathbf{q}}_m}{\partial x}\right] A_m\exp(-\mathrm{i}\omega_m t), \quad \text{and} \tag{16}$$

$$\frac{\partial^2\tilde{\mathbf{q}}_m}{\partial x^2} = \left[\mathrm{i}\frac{\mathrm{d}\alpha_m}{\mathrm{d}x}\hat{\mathbf{q}}_m + 2\mathrm{i}\alpha_m\frac{\partial\hat{\mathbf{q}}}{\partial x} - \alpha_m^2\hat{\mathbf{q}}_m\right] A_m\exp(-\mathrm{i}\omega t). \tag{17}$$

Inserting this flow decomposition (also known as PSE Ansatz) into the governing equations (2), and (3), subtracting the terms corresponding to the mean flow (discussed in the previous section) and introducing the simplifications discussed above, we arrive at a parabolic system of equations for each frequency mode that can be recast as

$$L_m\hat{\mathbf{q}}_m = R_m\frac{\partial\hat{\mathbf{q}}_m}{\partial x} + \frac{\hat{F}_m}{A_m}, \tag{18}$$

with

$$L_m = A_0 + A_y\frac{\partial}{\partial y} + A_{yy}\frac{\partial^2}{\partial y^2} + \mathrm{i}\frac{\mathrm{d}\alpha_m}{\mathrm{d}x}B_0 + \mathrm{i}\alpha_m B_1 + \alpha_m^2 B_2, \quad \text{and} \tag{19}$$

$$R_m = C_0 + 2\mathrm{i}\alpha_m C_1. \tag{20}$$

The matrix operators $A_0, A_y, A_{yy}, B_0, B_1, B_2, C_0$ and C_1 depend linearly on the mean flow quantities and on ω_m. The nonlinearities corresponding to interactions between different frequency modes and with the mean flow are gathered in the forcing term $\hat{F}_m$, and will be discussed later.

The system of equations (18) requires of an additional condition to be solvable, as the changes in the fluctuations can be absorbed either in the amplitude factor or the shape function. A normalization condition need be imposed to ensure that the shape functions only capture slow variations, and that fast oscillations and amplitude growth are captured by the amplitude factor. The condition devised by Herbert (1997) and then adapted by Cheung and Zaki (2011) is also adopted here

$$\int_0^1 \bar{\rho}\hat{u}_m^*\frac{\partial\hat{u}_m}{\partial x} + \bar{\rho}\hat{v}_m^*\frac{\partial\hat{v}_m}{\partial x} + \hat{\phi}_m^*\frac{\partial\hat{\phi}_m}{\partial x}\,\mathrm{d}y = 0. \tag{21}$$

Equations (18) and (21) defined the Parabolized Stability Equations (PSE) and are solved iteratively, the discretized version of the latter providing an update condition for the wavenumber α_m. At each iteration, the nonlinear terms $\hat{F}_m$ for each frequency and $\bar{F}$ for the mean flow are computed together in the time-domain, then Fourier-transformed back to the frequency domain.

PSE requires boundary conditions and inlet conditions for its closure. Wall boundary conditions analogous to those imposed in the PNS solution are also imposed here. The inlet fluctuation profile for each frequency is computed from a locally-parallel spatial stability problem derived from the PSE system of equations, as explained next.

2.5 SPATIAL LINEAR STABILITY EIGENVALUE PROBLEM

A linear stability eigenvalue problem can be obtained from the PSE, by introducing the most constrained assumption of locally-parallel flow. Under this simplification, the axial variation of the mean flow components is assumed to be so slow that first-order derivatives of the mean flow can also be neglected. The wavenumber then is not a slowly varying function of x, but a constant value that describes the *local* behavior of the linear instability waves, which leads to an instability eigenmode analysis. The modal perturbations now take the shape

$$\tilde{\mathbf{q}}_m = \check{\mathbf{q}}_m\exp\left(\mathrm{i}\alpha_m x - \mathrm{i}\omega_m t\right), \tag{22}$$

and the PSE equations are transform into the eigenvalue problem:

$$L_m\hat{\mathbf{q}}_m = \mathrm{i}\alpha_m R_m\hat{\mathbf{q}}_m. \tag{23}$$

Table 1. Comparison of the asymptotic interface height h_a, peak axial velocity U_{max} and development length L_d, for $h_{in} = 0.725$. CPU-times and spatial resolution corresponding to present computations are also given.

Case	L_d	h_a	U_{max}	CPU-time (seconds)
Asymptotic	-	0.558	1.743	-
Gada and Sharma (2012), $L = 70$	47.67	0.563	1.738	-
$\Delta x = 5 \cdot 10^{-2}$, $N_y = 51$	49.02	0.5639	1.70613	29
$\Delta x = 1 \cdot 10^{-2}$, $N_y = 51$	49.09	0.5640	1.70612	127
$\Delta x = 5 \cdot 10^{-2}$, $N_y = 101$	49.55	0.5605	1.72521	57
$\Delta x = 1 \cdot 10^{-2}$, $N_y = 101$	49.63	0.5602	1.72516	290
$\Delta x = 5 \cdot 10^{-2}$, $N_y = 201$	52.12	0.5578	1.73805	78
$\Delta x = 1 \cdot 10^{-2}$, $N_y = 201$	52.15	0.5578	1.73791	516

For each frequency ω_m, equation (23) delivers a complete eigenspectrum of modal solutions, characterized by the eigenvalues $\alpha_m^{(k)}$ and eigenfunctions $\hat{\mathbf{q}}_m^{(k)}$. The imaginary part of $\alpha_m^{(k)}$ determines the asymptotic amplitude growth or decay of the mode k, thus determining the instability character of the flow and the physical mechanisms responsible for its instability. Linear instability analysis (23) is useful in providing physical insight on the origin of the interfacial instabilities, and represents the *spatial* equivalent of the *temporal* problem studied by Kuru *et al.* (1995); Boomkamp and Miesen (1997), amongst many others. In the present context, it also allow us to define the inlet conditions for the PSE integration.

3. NUMERICAL METHODS

The governing equations for the PNS (10-13) and PSE (18) are discretized in the same manner and solved simultaneously. Sixth-order finite differences are used for the discretization of the cross-stream direction, while an implicit Euler scheme is used for the spatial marching along the axial direction. For numerical reasons, the Heaviside and Dirac's functions are replaced in the computations by smoothed functions, following Sussman *et al.* (1994). The width of the resulting smoothed interface is chosen to be twice the grid spacing.

A Newton method is used in the advancement of the PNS equations, in order to treat nonlinear terms and adjust the axial pressure gradient $\bar{P}_x$ so the mass flow rate of the two fluids is preserved. PSE equations are advanced for each $x-$section, and iterated together with the PNS solution to adapt the nonlinear interaction terms as well as the axial wavenumber α_m for each frequency. The iteration at each cross-section is stopped when the residuals in the updates of $\bar{P}_x$ and α_m drop below some prescribed tolerance, typically $tol = 10^{-8}$.

The eigenvalue problem (23) is solved using an in-house implementation of the shift-and-invert Arnoldi algorithm. This Krylov's subspace iteration allows the computation of an arbitrarily large window of the eigenspectrum at a small fraction of the cost of alternatives like the QZ algorithm.

Matrix operators are formed and operated on in sparse format. In-house routines are used for matrix-vector and matrix-matrix operations, while the ordering library METIS and the multifrontal solver library MUMPS (Amestoy *et al.* (2001)) are used for the computation of LU decompositions and back-substitutions. The use of sparse storage and operations reduces drastically the computational resources required for the solution as compared to an equivalent dense-algebra computation (Gennaro *et al.* (2013)). Required memory is reduced by an order of magnitude, while CPU is reduced further, thus allowing the computations to be done in a laptop computer and in times of minutes.

4. RESULTS

The oil/water flow on a two-dimensional channel is considered here. This case is chosen in order to compare with the numerical simulations by Gada and Sharma (2012), and has the twofold advantage of being a low-Reynolds, and thus the flow within each phase is mostly laminar, and of being representative of some practical applications. Gada and Sharma (2012) consider a set-up in which the two phases present an uniform velocity profile at the inlet with the same velocity, which is taken as the reference velocity U_1^*. The density and viscosity ratios are taken as $\chi = 1.218$ and $\eta = 0.1874$, respectively.The cases considered here correspond to $Re = 241.5$ and $Fr = 3.017$, and two different interface heights at inlet, namely $h_{in} = 0.725$ and 0.9. The effect of surface tension is neglected in the present computations. This has negligible effect on the base flow, and a small destabilizing effect on the perturbations, as compared to Gada and Sharma (2012). These parameters correspond, respectively, to steady stratified and self-sustained wavy stratified flow patterns.

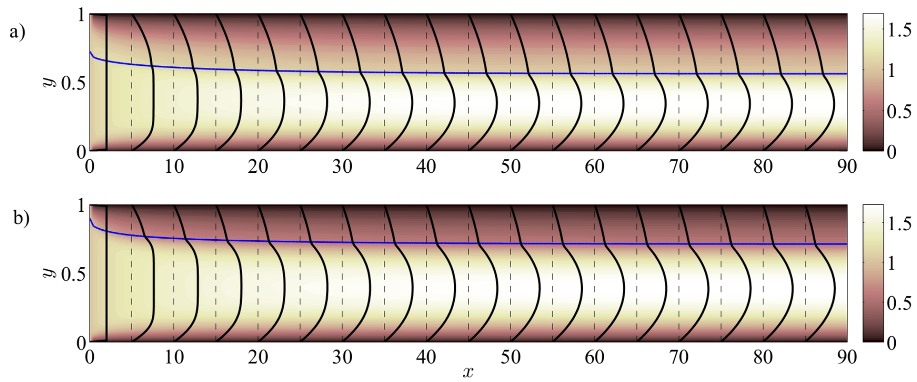

Figure 1. Mean flows computed as PNS solutions for $h_{in} = 0.725$ (a) and $h_{in} = 0.9$ (b). Streamwise velocity $\bar{u}$ contours are shown along with the corresponding velocity profiles. The velocity profile at each section x_c is plotted as $2\bar{u}(x_c, y) + x_c$, to ease visualization. Blue lines correspond to the interface location.

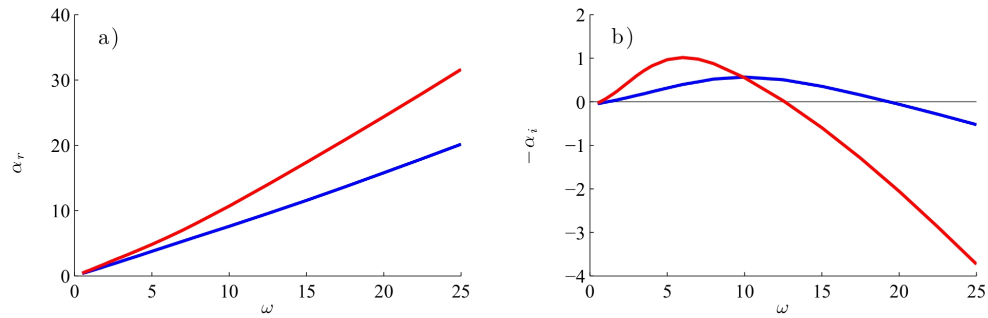

Figure 2. Linear stability analysis of the asymptotic flow profiles: axial wavenumber α_r (a) and spatial growth rate $-\alpha_i$ (b) versus ω, for cases $h_{in} = 0.725$ (blue) and $h_{in} = 0.9$ (red).

4.1 VALIDATION OF THE PNS COMPUTATIONS

The steady configuration is used for the validation of the PNS method employed in the computation of the mean flow. The downstream evolution of this flow converges to an asymptotic fully-developed flow in which the interface height and the velocity profile does not evolve along the axial direction anymore. This asymptotic solution can be computed as an analytical solution of a one-dimensional problem, i.e. the momentum conservation on the axial direction. This solution delivers a velocity profile with peak velocity equal to $U_{a,max} = 1.743$ and interface height $h_a = 0.558$. Gada and Sharma (2012) compare their simulation against the analytical solution, and also measure the development length L_d, defined as the axial length at which the computed U_{max} reaches 99% of the fully-developed value. Their results are sensitive to the axial domain extent, and show that they need to simulate a channel domain longer than $60H^*$ to converge the development length. Also, they require of a minimum 6000×100 resolution in order to obtain converged results.

Table 1 compares the development length, asymptotic interface height and peak velocity for the analytic solution, the computations of Gada and Sharma (2012), and the results of present computations with different resolutions. The computations are marched up to 70 channel widths downstream of inlet, and CPU times are also shown.

4.2 LINEAR STABILITY ANALYSIS OF THE ASYMPTOTIC FLOW

The spontaneous appearance of interfacial waves in the present set-up is necessarily associated with a linear instability of the steady flow computed by PNS. If the oscillations are to survive at long distances once the flow has developed, the underlying mean flow has to be linearly unstable. This linear stability analysis also predicts the range of frequencies that dominate the interfacial waviness, as well as estimations of the axial wavenumbers; these aspects are studied as a preliminary step to the PSE integration.

Figures 2 show the axial wavenumber α_r and spatial growth rate $-\alpha_i$ as a function of circular frequency ω for the asymptotic steady solutions for the two cases considered in this work, i.e. $h_{in} = 0.725$ ($h_a = 0.558$, $U_{max} = 1.743$) and $h_{in} = 0.9$ ($h_a = 0.706$, $U_{max} = 1.776$). The two asymptotic profiles are found to be linearly unstable for a relatively wide range of frequencies. This is in an apparent contradiction with the simulations by Gada and Sharma (2012), that recovered steady flow for the first of these conditions. However, it should be noted that linear instability is

Table 2. PSE computations for $h_{in} = 0.725$ and $\omega = 10$. The real and imaginary parts of the axial wavenumber α at $x = 90$ is compared for different spatial resolutions. The CPU-time for each case is also shown.

Case	Δ_x	N_y	α_r	α_i	CPU-time (seconds)
C1	$5 \cdot 10^{-2}$	101	7.59138	-0.55850	72
C2	$5 \cdot 10^{-2}$	201	7.56885	-0.57681	108
C3	$5 \cdot 10^{-2}$	301	7.56120	-0.58163	176
C4	$1 \cdot 10^{-2}$	101	7.59130	-0.55846	426
C5	$1 \cdot 10^{-2}$	201	7.56887	-0.57680	711
C6	$1 \cdot 10^{-2}$	301	7.56124	-0.58171	1096
C7	$5 \cdot 10^{-3}$	101	7.59130	-0.55843	862
C8	$5 \cdot 10^{-3}$	201	7.56888	-0.57679	1761
C9	$5 \cdot 10^{-3}$	301	7.56125	-0.58170	2340

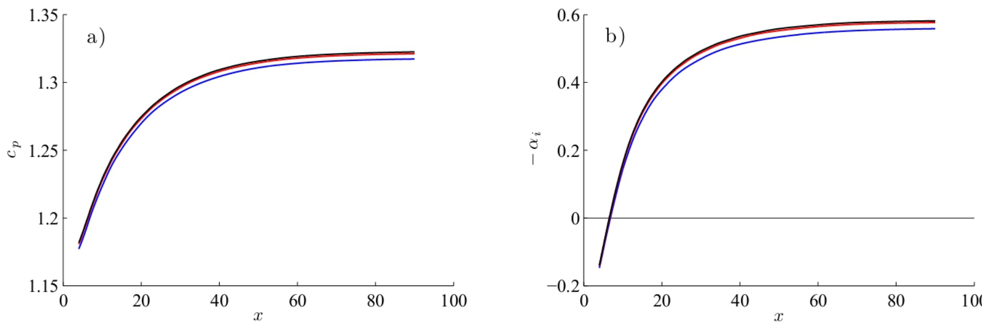

Figure 3. PSE computations for $h_{in} = 0.725$ and $\omega = 10$. Phase velocity $c_p = \omega/\alpha_r$ (a) and spatial growth rate $-\alpha_i$ (b) for $\Delta_x = 5 \cdot 10^{-2}$ and $N_y = 101$ (blue), $N_y = 201$ (red) and $N_y = 301$ (black).

not a sufficient condition for the persistence of interfacial waves in the absence of disturbances entering through the inlet section. The range of unstable frequencies is narrower for $h_{in} = 0.9$, but the peak spatial growth rate almost doubles that of $h_{in} = 0.725$, which might explain the change of pattern observed in the reference simulations.

4.3 SPATIAL EVOLUTION OF INTERFACIAL INSTABILITIES COMPUTED BY LINEAR PSE

The implementation of the linear PSE solution procedure is validated first, taking into account that it must recover asymptotically the spatial complex wavenumber α determined by the linear stability eigenvalue problem in the previous sub-section. In addition, the axial evolution of the wavenumber can be used to study the sensitivity of the computations to the spatial discretization. Table 2 shows the wavenumbers recovered in the PSE computations for the case $h_{in} = 0.725$, $\omega = 10$, at $x = 90$ for different resolutions, along with the CPU times for the coupled integration of the PNS and PSE equations up to that axial coordinate. Figure 3 shows the axial evolution of the wavenumber. In this case, the phase velocity $c_p = \omega/\alpha_r$ is used as its physical meaning is more evident. Results are shown to be nearly independent of the axial step size Δ_x, and to be reasonably converged with $N_y = 201$.

The downstream evolution of the perturbation field associated with interfacial instability is studied now for the two validation cases taken from Gada and Sharma (2012). The phase velocity and spatial growth rate as a function of the axial coordinate for the flows with $h_{in} = 0.725$ and $h_{in} = 0.9$ are shown in figures 4 and 5, respectively. The range of frequencies goes from $\omega = 1$ to 20, then comprising the most unstable ones. A significant difference appears between the two cases: while the flow with $h_{in} = 0.725$ is initially stable, becoming unstable for all frequencies in the range $\omega = 5 - 20$ at nearly the same axial coordinate ($x \approx 10$), for the flow with $h_{in} = 0.9$ all but the lowest frequencies are initially unstable. This can explain the different behavior of these flows observed in the numerical simulations by Gada and Sharma (2012): very small oscillations near the inflow due to adaptation of the inlet conditions will decay and vanish for $h_{in} = 0.725$, so there are no perturbations to be amplified by the linear instability when it sets in downstream. For $h_{in} = 0.9$, these small perturbations at inlet are amplified from the beginning, thus giving rise to observable interface waviness. The inclusion of the neglected surface tension would stabilize the instability waves, but is not expected to alter the qualitative behavior.

The influence of the mean flow spatial evolution on the interfacial waves is also observable in the phase velocities. For

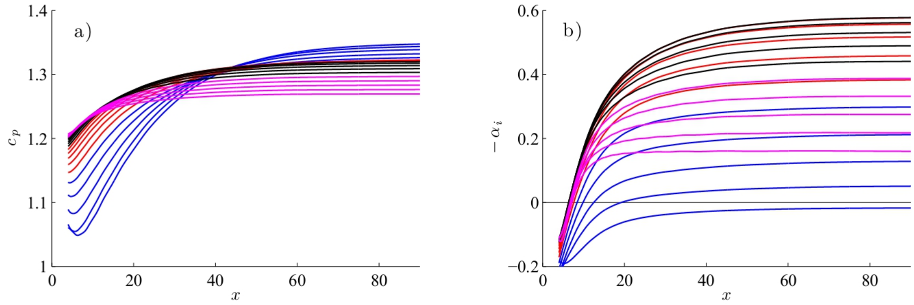

Figure 4. PSE computations for $h_{in} = 0.725$. Phase velocity $c_p = \omega/\alpha_r$ (a) and spatial growth rate $-\alpha_i$. Frequencies span from $\omega = 1$ (first blue) to 20 (last magenta) with a step of $\Delta\omega = 1$.

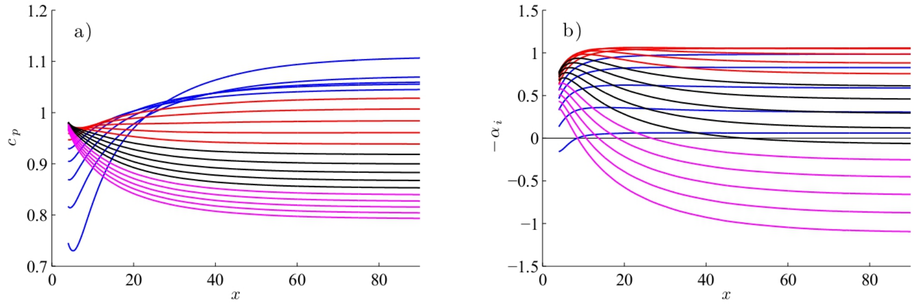

Figure 5. PSE computations for $h_{in} = 0.9$. Phase velocity $c_p = \omega/\alpha_r$ (a) and spatial growth rate $-\alpha_i$. Frequencies span from $\omega = 1$ (first blue) to 20 (last magenta) with a step of $\Delta\omega = 1$.

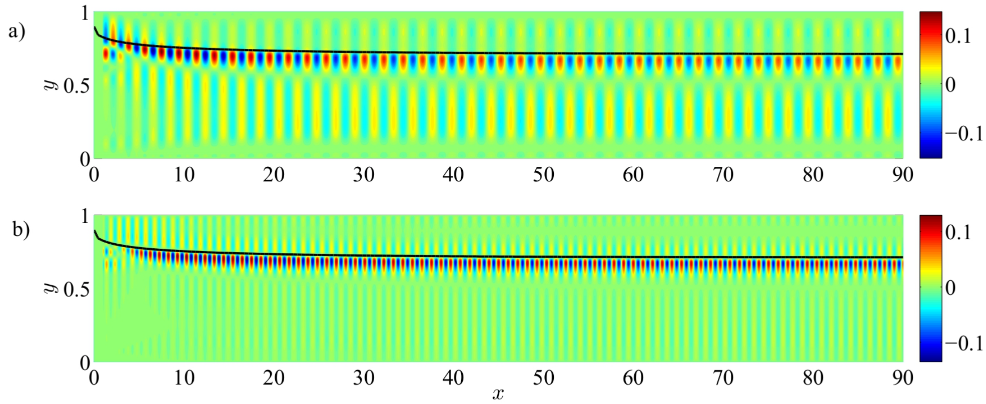

Figure 6. Streamwise velocity fields computed as linear PSE solutions for $h_{in} = 0.9$ at $\omega = 3$ (a) and $\omega = 6$ (b). The velocity field has been re-scaled at each x to eliminate the exponential spatial growth, in order to make the main features of the shape functions visible. Black solid lines correspond to the mean-flow interface location.

$h_{in} = 0.725$, the wave velocity for any of the frequencies considered increases downstream. Conversely, for $h_{in} = 0.9$, the phase velocity of the higher-frequency waves decreases gradually downstream. This qualitative change is related to the relative location of the critical layer on the cross-section, and illustrates how subtle changes in the development of the mean flow may alter the instability behavior, remarking the importance of an accurate mean flow solution.

Figure 6 shows the spatial structure of the streamwise velocity fluctuations for $h_{in} = 0.9$ and two different frequencies, $\omega = 3$ and 6. Note that $\omega = 6$ is approximately the frequency at which waves exhibit a larger linear amplification. In the reconstruction of the velocity field, equations (14) and (15) are used, but the imaginary part of α is zeroed. This is done in order to isolate the exponential spatial growth from the perturbation shape; otherwise, the growth of the fluctuations' amplitude would hide the main features of their shape. The instability waves are shown to have peak velocity fluctuations in the faster phase (water in this case), towards the interface, a result in agreement with the findings of Boomkamp and

Miesen (1997). The axial wavelength for the dominant frequency $\omega = 6$ is $L_x = 2\pi/\alpha_r \approx 2.2$ times the channel width, comparable to the fully nonlinear simulations by Gada and Sharma (2012) (figure 4(m) therein), from which a dominant wavelength $L_x \sim 2.4 - 2.8$ can be roughly inferred.

5. CONCLUDING REMARKS

A novel methodology for the prediction of interfacial instability of two concurrent phases flow along ducts has been presented. This methodology does not consider a cross-sectional average of the flow properties nor additional simplifications on the velocity profiles, as opposed to the mechanistic models typically employed in the literature. Conversely, the complete velocity field is computed by means of a parabolic integration along the axial direction. A level-set method for interface tracking is combined with parabolized Navier-Stokes equations and parabolized stability equations to provide an accurate description of the formation process of interfacial waves. The implementation of the method, using high-order finite differences in the cross-section and sparse linear algebra, enables the computation of the unsteady flow field in a channel with axial development of $O(100)$ times the channel width in few minutes on a laptop computer.

Validations of the proposed methodology have been performed against numerical results in the literature for laminar oil-water flows. Further developments in the code are underway to introduce the nonlinear coupling between the instability waves and their effect on the mean flow, that will be included in the final version of the paper and presented in the conference. Additional improvements of the model will include the implementation of eddy viscosity models to account for the extra viscous dissipation of smaller scales in turbulent flow and the extension of the methodology to ducts of arbitrary two-dimensional cross-section, with the objective of comparing with numerical simulations and experiments on air-water rectangular channels and circular pipes that are been carried out in the Department of Mechanical Engineering at PUC-Rio.

6. ACKNOWLEDGMENTS

This work is funded by the Science without borders/CAPES- “Attraction of Young Talents” Fellowship.

7. REFERENCES

Amestoy, P.R., Duff, I.S., L'Excellent, J.Y. and Koster, J., 2001. “A fully asynchronous multifrontal solver using distributed dynamic scheduling”. *SIAM J. Matrix Anal. Appl.*, Vol. 23, No. 1, pp. 15–41. ISSN 0895-4798.

Anderson, D.A., Tannehill, J.C. and Pletcher, R.H., 1984. *Computational fluid mechanics and heat transfer*. McGraw-Hill, 1st edition.

Barnea, D. and Taitel, Y., 1993. “Kelvin-Helmholtz instability criteria for stratified flow: viscous versus non-viscous (inviscid) approaches”. *Int. J. Multiphase Flow*, Vol. 19, No. 4, pp. 639–649.

Boomkamp, P.A.M. and Miesen, R.H., 1997. “Classification of instabilities in parallel two-phase flow”. *Int. J. Multiphase Flow*, Vol. 22, No. Suppl, pp. 67–88.

Cheung, L.C. and Zaki, T.A., 2011. “A nonlinear PSE method for two-fluid shear flows with complex interfacial topology”. *J. Comp. Physics*, Vol. 230, pp. 6757–6777.

Gada, V.H. and Sharma, A., 2012. “Analytical and level-set method based numerically on oil-water smooth/wavy stratified-flow in an inclined plane-channel”. *Numer. Heat Transfer B*, Vol. 56, pp. 307–322.

Gennaro, E.M., Rodríguez, D., Medeiros, M.A.F. and Theofilis, V., 2013. “Sparse techniques in global flow instability with application to compressible leading-edge flow”. *AIAA J.*, Vol. 51, No. 9, pp. 2295–2303.

Herbert, T., 1997. “Parabolized stability equations”. *Ann. Rev. of Fluid Mechanics*, Vol. 29, pp. 245–283.

Holmes, P., Lumley, J. and Berkooz, G., 1996. *Turbulence, Coherent Structures, Dynamical Systems and Symmetry*. Cambridge University Press.

Kuru, W.C., Sangalli, M., Uphold, D.D. and McCready, M.J., 1995. “Linear Stability of Stratified Channel Flow”. *Int. J. Multiphase Flow*, Vol. 21, No. 5, pp. 733–753.

Lin, P. and Hanratty, T., 1986. “Prediction of the Initiation of Slugs with Linear Stability Theory”. *Int. J. Multiphase Flow*, Vol. 12, No. 1, pp. 79–98.

Reynolds, W. and Hussain, A., 1972. “The mechanics of an organized wave in turbulent shear flow. Part 3. Theoretical models and comparisons with experiments”. *J. Fluid Mech.*, Vol. 54, pp. 263 – 288.

Sussman, M., Smereka, P. and Osher, S., 1994. “A level set approach for computing solutions to incompressible two-phase flow”. *J. Comp. Phys.*, Vol. 114, pp. 146–159.

Taitel, Y. and Dukler, A., 1976. “A Model for predicting flow Regime transitions in horizontal and near horizontal gas-liquid flow”. *A. I. Ch. E.*, Vol. 22, pp. 47–55.

8. RESPONSIBILITY NOTICE

The author is the only responsible for the printed material included in this paper.